European Journal of Pharmaceutics and Biopharmaceutics 141 (2019) 149–160

Contents lists available at ScienceDirect

European Journal of Pharmaceutics and Biopharmaceutics

journal homepage: www.elsevier.com/locate/ejpb

Research paper

Holistic QbD approach for hot-melt extrusion process design space evaluation: Linking materials science, experimentation and process modeling

Rachel C. Evans[a,b], Esther S. Bochmann[a,b], Samuel O. Kyeremateng[a], Andreas Gryczke[a], Karl G. Wagner[b,*]

[a] Drug Product Development, AbbVie Deutschland GmbH & Co. KG, Ludwigshafen, Germany
[b] Department of Pharmaceutical Technology and Biopharmaceutics, University of Bonn, Bonn, Germany

ARTICLE INFO

Keywords:
Hot-melt extrusion (HME)
Quality-by-design
Design space
Amorphous solid dispersion (ASD)
Numerical simulation
Melt viscosity

ABSTRACT

The aim of this work was to investigate the relationship between formulation material properties, process parameters and process performance for the manufacturing of amorphous solid dispersions via hot-melt extrusion (HME) using experimentation coupled with process modeling. Specifically, we evaluated the impact of the matrix copovidone melt rheology with and without the addition of a plasticizing surfactant, polysorbate 80, while also varying the process parameters, barrel temperature and screw speed, and keeping fill volume constant. To correlate the process performance to a critical quality attribute, we used telmisartan as an indicator substance by processing at temperatures below its solubility temperature in the polymeric matrix. We observed a broader design space of HME processes for the plasticized formulation with respect to screw speed than for the copovidone-only matrix formulation. This observation was determined by the range of observed melt temperatures in the extruder, both measured and simulated. The reason was not primarily linked to a reduced shear-thinning behavior, characterized by the power law index, n, but instead more to an overall reduced melt viscosity during extrusion and zero-shear rate viscosity, η_0, accordingly. We also found that the amount of residual crystallinity of telmisartan correlated with the simulated maximum melt temperature in the extruder barrel. This finding confirmed the applicability of the temperature-dependent API-matrix solubility phase diagram for HME to process development. Given the complex inter-dependent relationships between material properties, process and performance, process modeling combined with reduced laboratory experimentation was established as a holistic approach for the evaluation of Quality-by-Design-based HME process design spaces.

1. Introduction

Hot-melt extrusion (HME) is a complex, commonly researched and commercialized technique used for the production of amorphous solid dispersions (ASD) of poorly-water soluble active pharmaceutical ingredients (APIs) [1–3]. Generally, the process involves several interrelated steps which can be considered sub-unit operations within the extruder barrels. Typically a co-rotating twin-screw extruder (TSE) is used for pharmaceutical applications [4]. Usually, a powder-based mixture composed of API and at least one polymer matrix is fed at controlled feed rate into the TSE onto rotating screws containing at least one section of mixing elements. Melting or softening of the matrix occurs due to heat rise resulting from conduction from the barrel housing or by viscous dissipation from the shear imparted by conveying and mixing screw elements. Ideally, through this mixing and temperature rise, the API melts or dissolves into the matrix and distributes to form a homogeneous single phase with the matrix, e.g. an ASD. Lastly, the material may be degassed prior to being extruded through the die, formed and cooled.

The complex nature of HME and the transformation of the input material through extrusion can be captured by the application of the materials science tetrahedron (MST). The MST origin and applicability to drug product development was explained with several examples by Sun, primarily focusing on tablet compression [5]. Here, the concept is interpreted and applied for HME and presented in Fig. 1. The corners of the tetrahedron are represented by the material structure, material properties, process parameters and process performance. Like interstitial sites in a crystal lattice, characterization and process simulation

* Corresponding author at: Gerhard-Domagk-Strasse 3, 53121 Bonn, Germany.
E-mail address: kgwagner@uni-bonn.de (K.G. Wagner).

https://doi.org/10.1016/j.ejpb.2019.05.021
Received 12 March 2019; Received in revised form 22 May 2019; Accepted 24 May 2019
Available online 24 May 2019
0939-6411/

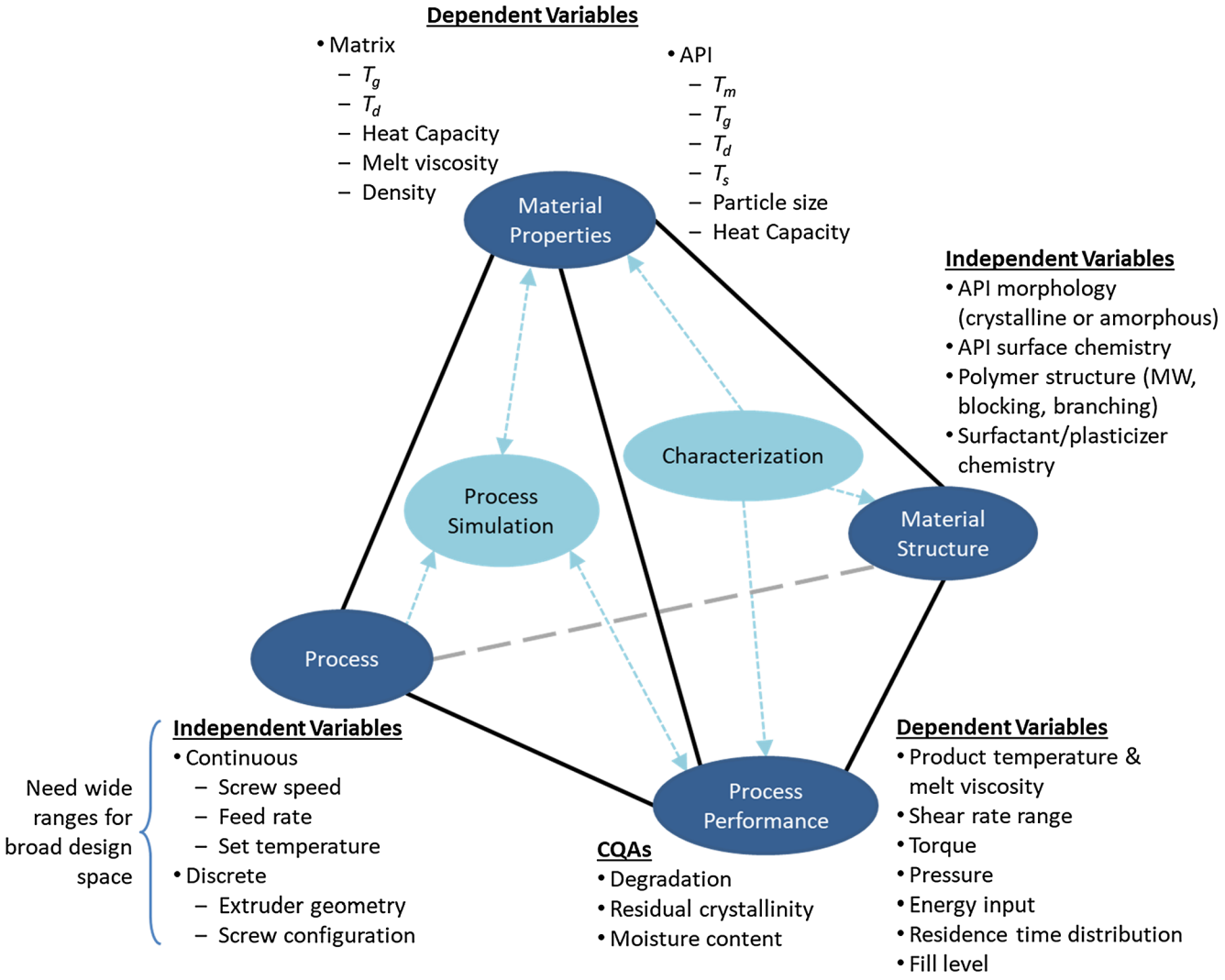

Fig. 1. The materials science tetrahedron as applied to hot-melt extrusion for ASD formation. T_g = glass transition temperature, T_m = melting temperature, T_d = degradation temperature, T_s = solubility temperature (temperature at which a given concentration of API is thermodynamically soluble in the matrix).

are placed at the core of the tetrahedron. The value in describing a process using the MST is that all of the inter-dependent relationships can be holistically described and analyzed.

Inherent to any process, variation of several independent and dependent variables influence the final material produced by the process. In HME, the independent variables are both continuous and discrete. Continuous independent variables in HME are the screw speed, feed rate, barrel temperature and vent pressure. Discrete independent variables are the extruder scale, screw configuration, barrel length, die geometry and API and matrix properties. When an HME process is analyzed via a design of experiments (DoE), a regression equation describing the relationship between a given response and the independent variables typically contains terms with not only main effects but also interactions [6]. The existence of these interactions suggests that the more important factors in the process may be dependent variables. Dependent variables for HME have been identified as the product temperature and melt viscosity, shear rate, torque, pressure, energy input and residence time distribution [7,8]. Process performance responses are typically defined by the critical quality attributes of the product (CQAs), the most important of which are the residual crystallinity and degradation as they determine the amount and form of solubilized API available to contribute to enhanced bio-performance. Other important CQAs also include assay and uniformity, as well as moisture content, which is important for physical and potentially chemical stability of an ASD.

In addition to the influence of process parameters, the raw material properties of a given formulation, especially their thermal properties, determine processing behavior and potentially also the product's final quality. The right material properties will enable optimal processing with a broad design space and optimal product quality and vice versa. Knowledge and understanding of the material properties and their significance can facilitate working with and not against the natural behavior of the formulation. For HME, understanding the thermal properties and the role of the matrix rheological properties is essential to designing and controlling the process and the resulting product quality. Specifically, some of the most important material properties are the initial API particle size, matrix polymer and API glass transition temperatures (T_g), the API melting and solubility temperatures (T_m and T_s), the API and matrix degradation temperatures (T_d), and the matrix melt viscosity as a function of temperature and shear rate. In addition to being a function of temperature and shear rate, the matrix melt viscosity can also be a function of additional components incorporated within it, such as moisture content, undissolved and dissolved API, surfactant and plasticizer, depending on relative concentrations [9–28]. Characterization of the matrix T_g and melt viscosity have been investigated to identify the minimum processing temperature and extruder torque limitation [29–31,9,32,10,33,34].

Because the formation of an ASD via HME involves physical

transformation of the raw materials, the material properties of the product being processed can change as a function of the position along the length of the extruder. For example, an API with T_g much lower than that of the matrix will plasticize the matrix upon dissolution and mixing [26]. This effect will reduce the viscosity and therefore reduce viscous dissipation. However, an API can also anti-plasticize the matrix if its T_g is higher than that of the matrix, leading to potentially more viscous dissipation [35]. Based on these complex and inter-dependent relationships between the material properties and the process, and the evolution of the material properties that occurs during processing, a thorough understanding of both the thermodynamic [36,37] and melt viscosity properties of the materials is essential. It should not be neglected that the raw material properties can be dependent upon their structure [37]; however, this relationship is less central to the topic of this research and is therefore not discussed beyond the presentation in Fig. 1.

Knowledge of the material properties and their relationship to processing characteristics is fundamental to the successful development of broad design spaces and implementation of Quality-by-Design (QbD) [38]. In addition to building relationships via laboratory experiments, process modeling can help to establish the relationships within the tetrahedron and to provide deeper insight. Process models take into account the relevant properties of the material being processed in relation to the process parameters and equipment geometries, even accounting for evolution of the properties as a function of location in the process and feeding that back into the computation by way of numerical methods. Upon variation of any input parameter, process models are particularly useful for the generation of qualitative estimates and rank ordering, identifying the most influential variables. In this way, better experiments can be designed upfront, with perhaps a reduced number of variables to be tested. In addition, a synergistic approach utilizing both process modeling and relevant experimentation can yield answers to the gaps in understanding on both sides [39]. With a validated model, gaps in experimental data can be supplemented with simulated data or design spaces can be supported. However, because not all experimental factors can be modeled, at least not at the present, quantitative predictions are not always feasible for every scenario. In the end, the requirements of QbD can be fulfilled by a combination of experimentation and modeling to rationally select formulation components based on their material properties to ensure product performance, quality, and even processing performance.

Process modeling has been applied to twin-screw extrusion through the development of a number of 1D simulation software programs [40–43] and a number of studies in the polymer and food industries have been reported [44–54]. However, scholarly articles applying it to pharmaceutical HME are still limited. In our group, it has been used to optimize screw configurations during scaling, study and optimize sources of heat generation upon scaling, and simplify and ease the use of HME simulation in early-stage formulation development [32,55–57]. Other researchers have focused on performing 3D simulations based on smoothed particle hydrodynamics, reducing them to 1D models with the goal of applying them to pharmaceutical HME [58–62]. Studies specifically related to the modeling of pharmaceutical HME include, for example, the development of a new model of the residence time distribution and the time to dissolution [63,64].

The objective of this work was to study the influence of matrix melt viscosity, varied by the addition of a plasticizing surfactant, on the HME process design space. Specifically, the zero-shear rate viscosity, η_0, and the power law index, n, were regarded as both parameters were hypothesized to be impacted by the presence of a plasticizing surfactant. With the understanding that the power law index relates to a material's tendency for shear-thinning [52], we hypothesize that the processing design space with respect to screw speed for a formulation with surfactant present should be less sensitive to screw speed and therefore more broad. The objective for our work was to test this hypothesis in order to better understand the role of the matrix rheological properties in HME while simultaneously relating the findings to a measurable CQA, namely residual crystallinity. Because of this latter objective, out of scope was the generation of a crystal-free ASD; we instead explored a processing space within which we would be able to utilize residual crystallinity of the API telmisartan as an indicator for the process. The reasons for focusing on residual crystallinity are two-fold. First, the primary objective of solubility enhancement via the formation of an ASD is to break down the crystal lattice and transform the crystalline API into an amorphous form. Second, degradation of the API is also an important CQA, but as has been observed in a few cases, this may not occur until the API has first dissolved [6,65]. In addition, any analysis of the solubility enhancement of the model API as a result of formation of an amorphous form, as an ASD or not, was also out of scope, as this has already been demonstrated [35,66,67]. Along with the analysis of the rheological properties of our model system, and in order to fully interpret our findings, we also related the CQA results back to the thermodynamic properties, that is, the temperature-dependent API solubility phase diagram. Lastly, we used process simulation to gain access to non-measurable processing characteristics for additional interpretation of our findings.

2. Experimental

2.1. Materials

Telmisartan (TEL) was purchased from Molekula GmbH (Munich, Germany), polysorbate 80 Ph.Eur./NF (Tween 80, TW80) was purchased from Merck KGaA (Darmstadt, Germany) and vinylpyrrolidone-vinyl acetate copolymer (copovidone, Kollidon® VA 64, COP) was purchased from BASF SE (Ludwigshafen, Germany). All materials were used as supplied unless otherwise noted. Telmisartan displayed needle shaped morphology with a particle size less than 50 μm.

2.2. Methods

2.2.1. Determination of model system thermal properties

Thermal decomposition of TEL and TW80 was determined by thermogravimetric analysis (TGA) in 40 μL aluminum pans with 5–20 mg of substance, heating from room temperature to 300 °C with a heating rate of 10 K/min under nitrogen gas flow. TGA experiments were performed using a TGA/DSC 1 (Mettler-Toledo, GmbH, Giessen, Germany) with a Ministat 125 (Huber Kältemaschinenbau AG, Offenburg, Germany).

Basic thermal analysis such as thermal decomposition, melting temperature (T_m) and glass transition temperature (T_g) were performed. The T_m of TEL, taken as the peak of the melting endotherm, was confirmed using differential scanning calorimetry (DSC) by heating 4 mg of substance in 20 μL pierced aluminum pans and heated from room temperature to 280 °C at 10 K/min under nitrogen gas flow. The T_g of amorphous TEL, taken as the midpoint in the transition, was measured in the second heating after the T_m determination, holding the sample above the melting point for 1 min, then rapidly cooling at 50 K/min to −40 °C, and re-heating to the melting temperature at 10 K/min.

In addition, the solubility phase diagram of TEL in binary and ternary mixtures of COP and TW80 according to method in Kyerematen et al., was also generated [68]. The T_g of various mixtures was calculated using the Fox equation [69]. Physical mixtures for the API solubility phase diagram generation were cryomilled using a Sample Prep Freezer/mill 6770 (Spex, Stanmore, UK) with 5 min precooling and 1 min milling at 10 cycles per second.

DSC experiments were performed using a DSC 1 with auto-sampler (Mettler-Toledo, GmbH, Giessen, Germany) with a TC100 immersion cooler (Huber Kältemaschinenbau AG, Offenburg, Germany). Calibration of temperature for the DSC was performed with zinc and indium standards.

2.2.2. Sample preparation for extrusion

All compositions are in units of %w/w but are sometimes expressed as % to simplify naming of the various formulations.

2.2.2.1. Preparation of the matrices. Copovidone powder was dried in a vacuum oven VDL 115 (Binder GmbH, Tuttlingen, Germany) at 40 °C for approximately 3 days to reduce the moisture content prior to blend preparation.

A placebo mixture of 5.5 %w/w TW80 in COP was prepared using a 26 mm, 24L/D co-rotating twin screw extruder with vacuum vent prior to die, screw configuration composed of conveying and kneading disk elements with 2 mixing-zones, calender and cooling belt (ZSK26 MegaCompounder with W110, Coperion GmbH, Stuttgart, Germany). The concentration of TW80 reduced to approximately 5 %w/w when 10 %w/w TEL was added to the extruded matrix.

The calendered material was milled using an impact mill (UPZ100, Alpine Bau GmbH, Wals bei Salzburg, Austria) with rotor speed 12000 rpm, 1 mm round-hole screen. To ensure particle size distribution similarity to the dried COP, the milled extrudate was further sieved and only the fraction less than 200 µm was used for further processing. To confirm similarity in matrix particle size, the particle size distribution of both the COP and milled and screened TW80/COP extrudate were measured using a Mastersizer 3000 laser diffraction instrument with dry powder dispersion module (Malvern Instruments GmbH, Herrenberg, Germany). Approximately 2–5 g of material was measured 3 times for 30 s each, fed using the vibratory feeder and dispersed with 2 bar air pressure keeping the obscuration level between 2 and 8%, and measurements were analyzed according to the Fraunhofer approximation and averaged.

2.2.2.2. Blending of the matrices with TEL for extrusion. Blends of 10 % w/w TEL in either dried COP or milled and sieved TW80/COP extrudate were prepared by a blending-sieving-blending process to produce a uniform blend and minimize agglomerates of the API observed in the neat drug substance. The mixtures, 2 kg batch size, were blended for 2 min at 15 rpm in a 10 L bin (LM 40, L. B. Bohle Maschinen + Verfahren GmbH, Ennigerloh, Germany), discharged and hand-sieved through a 500 µm screen, re-charged to the bin and blended for a further 10 min at 15 rpm.

The moisture content of the blends was measured prior to extrusion via loss-on-drying (LOD) using a HB43-S moisture analyzer (Mettler-Toledo GmbH, Giessen, Germany). Approximately 5.5–6 g of blend was heated to 105 °C and held until mass was constant within ± 1 mg for 100 s. The bulk density of the blends was also calculated from the mass and bulk volume occupied by the aerated powder filled into a 250 mL graduated cylinder.

2.2.2.3. Extrusion of telmisartan blends. Both blends were extruded under a set of identical processing conditions (Table 1) using an 18.2 mm, 28 L/D co-rotating twin screw extruder (ZSK18 MegaCompounder, Coperion GmbH, Stuttgart, Germany). The screw configuration contained two zones with forward (green) and reverse (red) 60° kneading disks (Fig. 2) and vacuum vent ports prior to 1st mixing zone and prior to the die. The extruder barrel was composed of 7 temperature zones plus die set to 20/80/120/T/T/T/T/T °C, with T meaning target temperature. The target temperature was varied together in the experiment and is referred to as "barrel temperature." The screw speed and feed rate were varied together in order to maintain the same degree of fill in the extruder barrel using the simple specific feed load equation of mass flow rate divided by screw speed [70].

Table 1
Extrusion experiment design.

Parameter	Set points
Barrel and die temperature [°C]	170, 190, 200
Screw speed [rpm]*	100, 400
Feed rate [kg/hr]*	0.5, 2.0
Formulation	10% TEL/COP, 10% TEL/5% TW80/COP

* Feed rate and screw speed were adjusted together to maintain constant fill level.

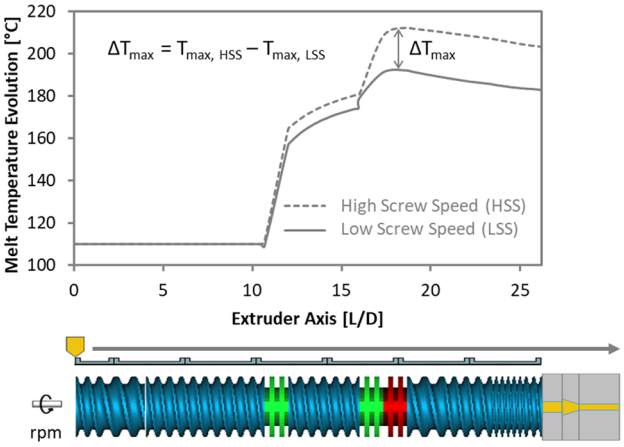

Fig. 2. Schematic representation of the melt temperature evolution along the screw profile from simulated data and calculation of ΔT_{max}. Note: die channel (light orange) is not to scale in relation to the screw diameter. (For interpretation of the references to color in this figure legend, the reader is referred to the web version of this article.)

The melt temperature at die exit, selected as the hottest temperature of the melt strand, was measured using a Testo 882 adjustable focus thermal imager (Testo SE & Co. KGaA, Lenzkirch, Germany).

Thin strands of extrudate were collected, separated from one another, and allowed to cool to room temperature before storage in air tight bottles. Samples were milled in a coffee grinder-type mill and sieved and powder less than 500 µm was used for further analysis and characterization.

2.2.3. Sample characterization of blends and extrudates

2.2.3.1. X-ray powder diffraction (XRPD). The residual crystalline TEL in milled extrudate samples was measured using an Empyrean system (PANalytical, Almelo, the Netherlands) using Cu K_α (45 kV and 40 mA), over an angular range of 5-8° 2θ with a step size of 0.026° 2θ. Data was analyzed using X'Pert High Score v4.1, including background subtraction on all diffraction patterns. Peak intensities at 6.75° 2θ were compared to those measured in a calibration set of samples with spiked crystallinity concentrations ranging between 0 and 10 %w/w. The residual crystallinity is reported as %w/w of sample.

2.2.3.2. Thermal properties for simulation. The heat capacity, c_p, of milled TEL extrudates with less than 1 %w/w residual crystallinity was measured by modulated DSC TA Q2000 (TA Instruments, Eschborn, Germany). Approximately 4 mg was placed in a pierced Tzero hermetic aluminum pan and heated to 100 °C, held for 2 min, cooled to 10 °C, held for 5 min, and then heated to 230 °C with a heating rate of 2 K/min with modulation ± 1 °C every 120 s. The instrument was temperature calibrated with gallium, indium, tin and bismuth standards. Calibration of the heat capacity was performed with a sapphire calibration standard. The thermal conductivity for both solid and liquid phases was assumed to be temperature independent and a literature value similar to other amorphous polymers was used [71]. The T_g of the respective formulation taken from the phase diagram was used as the input value for melt temperature in the Ludovic® simulation.

2.2.3.3. Density characterization for simulation. The solid density input parameter required for simulation was taken to be the bulk density of the starting blend, method described in Section 2.2.2.2. The melt

density was taken as the room temperature density calculated from disks made with a 20 mm diameter vacuum compression molding device (MeltPrep GmbH, Graz, Austria) [72].

2.2.3.4. Melt rheology. Melt viscosity of copovidone and the two TEL-containing formulations was measured using small angle oscillatory shear (SAOS) rheometry according to the method described by Bochmann et al., with minor modifications [73] noted here. Using milled extrudates with less than 1 %w/w residual crystallinity, sample disks were prepared using the 20 mm diameter vacuum compression molding device to a uniform thickness of 2 mm. An oscillatory rheometer (Haake® MARS® II, Thermo Fisher Scientific, Karlsruhe, Germany) was used with a 20 mm diameter plate-plate geometry and gap height of 2 mm. The melt viscosity was measured over a range of 150–180 °C, frequency sweep data was subsequently processed by time temperature superposition (TTS) to generate master curves. The master curves and obtained TTS data were fitted using the Carreau-Yasuda (C-Y) and Williams-Landel-Ferry (WLF) equations (see discussion below). The parameters of the fit to the reference temperature of 170 °C were then used as inputs to the Ludovic® simulation software. The master curves are presented as a function of angular frequency, which is equivalent to shear rate because the Cox-Merz relation has been found to apply to particle-free COP-based melts [73,74].

For modeling the melt viscosity, the Carreau-Yasuda [75,76] equation was selected to capture the non-Newtonian behavior of the polymer melts, specifically the shear rate dependency. The basic form of the C-Y equation expressing the melt viscosity as a function of shear rate is shown in Eq. (1):

$$\eta = \eta_{\infty} + (\eta_0 - \eta_{\infty})\cdot[1 + (\lambda\dot{\gamma})^a]^{\frac{n-1}{a}} \quad (1)$$

where η is the viscosity as a function of temperature and shear rate, $\dot{\gamma}$, η_0 is the viscosity at zero-shear rate, η_∞ is the viscosity at infinite shear rate, λ is the characteristic time, n is the power law index and a is the Yasuda constant.

If η_∞ is assumed zero, the equation simplifies to Eq. (2):

$$\eta = \eta_0\cdot[1 + (\lambda\dot{\gamma})^a]^{\frac{n-1}{a}} \quad (2)$$

The zero-shear rate viscosity, η_0, is both a function of the composition and the temperature of the material, and has been shown to correlate with T_g [11]. The power law index, n, describes the extent of shear-thinning that can occur for a given material [77,12] and has a value of 1 for Newtonian behavior and a value between 0 and 1 for materials exhibiting shear-thinning behavior.

Both the zero-shear rate viscosity, η_0, and the characteristic time, λ, are strong functions of temperature for amorphous pharmaceutical polymers, especially near the T_g of the polymer, roughly $T_g < T < T_g + 100$ °C. The temperature dependency can be accounted for by use of the WLF equation [52,78,79] (equation (3)):

$$\log(a_T) = \frac{-C_1(T - T_0)}{C_2 + (T - T_0)} \quad (3)$$

where a_T is a shift factor resulting from time-temperature superposition processing of rheological data, T is the target temperature, T_0 is the reference temperature, and C_1 and C_2 are constants. Eqs. (4) and (5) are used to calculate the melt viscosity and characteristic time at temperatures other than the reference temperature:

$$a_T = \frac{\eta_T}{\eta_0} \quad (4)$$

$$a_T = \frac{\lambda_T}{\lambda_0} \quad (5)$$

where the subscripts T and 0 refer to the desired and reference temperatures, respectively.

2.2.4. Process simulation with Ludovic® software

Process simulations of the laboratory experiments on the ZSK18 were performed using Ludovic® v.6.1 software (Sciences Computers Consultants, Saint Etienne, France). Ludovic® is a 1D numerical simulation software representing the polymer flow in a hot-melt co-rotating twin-screw extrusion process. The extruder geometry, polymer material properties and extrusion process parameters are all inputs for the computation. The Ludovic® model, its development and working principles have been summarized elsewhere [41,55,56]. Briefly, temperature and pressure are computed locally in discretized c-shaped chambers, and computation proceeds backward from the die until the convergence criteria of product temperature equals the defined melting or softening temperature, the pressure is equal to zero, and no further restrictive elements are present upstream. The numerical computations are performed iteratively because the fill volume is unknown for starve-fed extruders. The iteration begins with a user-defined exit temperature, in our case chosen to be that of the die temperature.

Additional parameters describing the ZSK18 extruder needed for simulation are: center line of 15 mm, screw/barrel leakage of 0.14 mm, and 10 mm diameter die opening. The screw configuration, composed of conveying elements of various pitch, forward 60° kneading blocks shown in green and reverse kneading block shown in red, is displayed at the bottom of Fig. 2.

Sensitivity analysis of the Ludovic® model with varied rheological parameters, n and η_0 in the Carreau-Yasuda equation, were performed to determine the relative impact of n and η_0 on melt temperature evolution. Copovidone was used as the baseline material with n and η_0 ranges selected within that of previously measured values when the formulation was varied by addition of surfactant. Copovidone at a reference temperature of 150 °C has $n = 0.577$ and $\eta_0 = 61000$ Pa·s. The extruder and screw geometry used for this study was the same as for all other simulations of the ZSK18 extruder. The barrel temperature was varied along with the screw speed, and the feed rate was adjusted in combination with the screw speed to maintain constant fill level. The thermal exchange coefficients used were 500 W/m^2·K in the barrel and 500 W/m^2·K in the die.

Process simulations at conditions identical to the TEL experimental extrusion conditions were performed to validate the model for telmisartan-containing formulations. The model was validated by correlating the melt temperature at die exit, measured experimentally, with that of the simulated value. The thermal exchange coefficients used were 300 W/m^2·K in the barrels and 100 W/m^2·K in the die.

In addition to the melt temperature at die exit, the maximum melt temperature along the screw and the total viscous dissipated energy from the screw were analyzed. The effect of screw speed on melt temperature evolution was quantified by calculating the difference in maximum melt temperature, ΔT_{max} in this case corresponding with a position in the reverse kneading block, in red color (Fig. 2), between high and low screw speeds. The total viscous dissipated energy in the screw is calculated by Ludovic® as the sum of the viscous dissipated energy computed in each c-shaped chamber, utilizing the local values of computed shear rate, viscosity, discretized volume and local residence time for computation.

3. Results

3.1. Selection of model system – Material properties

In order to test our hypothesis that the processing design space with respect to screw speed should be broader with plasticizing surfactant present, an appropriate model system needed to be identified. Such a system would require unique material properties for both the model API and surfactant with plasticizing behavior. To focus on the plasticization induced by the surfactant, the selected API should not substantially alter the T_g of the matrix polymer. In addition, the API should not be highly soluble in the polymer matrix, in order to monitor residual

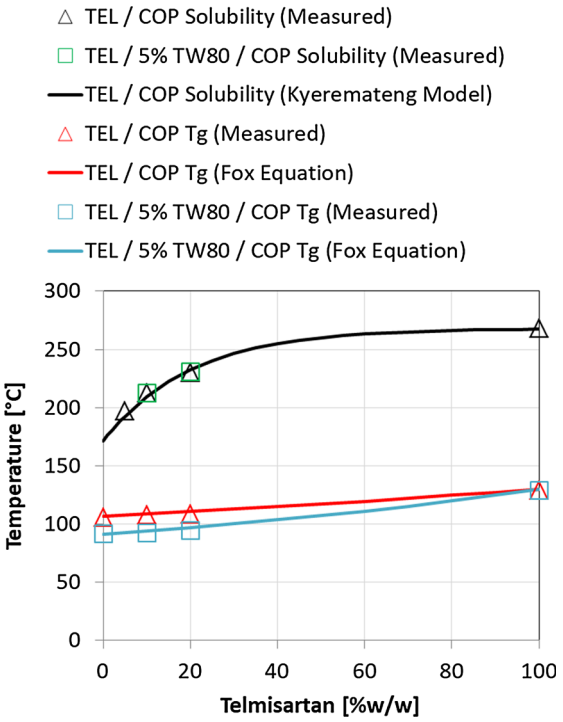

Fig. 3. Phase diagram of telmisartan/copovidone, with and without TW80. Black line is the solubility curve and indicates the temperature at which a given concentration of TEL is soluble in the polymer matrix. The red and blue lines indicate the glass transition temperature as a function of the concentration of TEL in a COP matrix or a 5% TW80/COP matrix, respectively. (For interpretation of the references to color in this figure legend, the reader is referred to the web version of this article.)

crystallinity, and should be thermally stable as degradation could also potentially alter the viscosity of the system. The surfactant should also be thermally stable and non-volatile, not alter the API's solubility in the overall matrix, and be miscible at the selected concentration. After screening of various APIs and surfactants to meet these criteria, telmisartan was selected as model API, polysorbate 80 (TW80) as model surfactant/plasticizer and copovidone (COP) as matrix polymer.

3.1.1. Thermal properties and phase diagram

TEL is thermally stable and exhibited moderate solubility in COP and COP/TW80 matrices, independent of the matrix composition up to 5 %w/w TW80. TEL melts at 269 °C, begins to thermally decompose at ~280 °C (data not shown) and has an amorphous T_g of 129 °C. According to the API solubility phase diagram, the API solubility temperature, T_s, of TEL in COP is unchanged when 5 %w/w TW80 is present (Fig. 3). Experimentally determined T_s at 20 %w/w TEL in matrices was used to construct the solubility curve according to the Kyerematen model and method [68]. Additional T_s data at 5 and 10 %w/w TEL were generated to independently confirm the predicted solubility by the model. Based on these results, 5 %w/w TEL should be soluble at 197 °C, 8 %w/w at 203 °C, and 10 %w/w at 213 °C. TEL thermal stability in

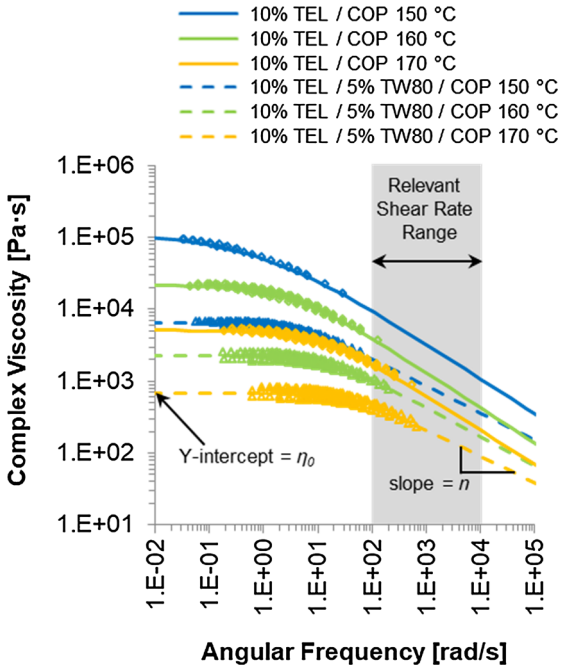

Fig. 4. Plotted master curves and TTS-shifted data points for both formulations as a function of temperature.

COP was confirmed by HPLC analysis of preliminary ASDs extruded at temperatures up to 230 °C (see supplementary data).

TEL had the tendency to anti-plasticize the COP or TW80/COP matrix, but at the 10 %w/w concentration used, the effect was minimal or even negligible. The matrix polymer, COP, had a dry T_g of 107 °C while the T_g of TEL was 129 °C. The measured T_g of 20 %w/w of TEL in COP was 108.5 °C. TEL exhibited a slight anti-plasticizing effect on COP, however, at 10 %w/w drug load, this effect was negligible as the T_g (107.8 °C) is close to that of COP. The T_g of the ternary system 20% TEL/5% TW80/COP was 95 °C, slightly lower than the binary mixture, indicating a plasticizing effect of the TW80. The T_g of the ternary system with 10% TEL/5% TW80/COP was 92 °C.

3.1.2. Blend powder properties

The blends were designed to be as identical as possible in terms of powder properties so as to provide a similar environment into which the TEL could incorporate and dissolve, albeit with different melt rheological properties. The properties of the matrix considered were the bulk density, the particle size distribution and the moisture content and were kept constant (Table 2).

3.1.3. Rheological properties

3.1.3.1. Model formulations. The melt viscosity as a function of angular frequency at reference temperatures of 150 °C, 160 °C and 170 °C of the two formulations, 10% TEL/COP and 10% TEL/5% TW80/COP, shows the plasticizing effect of the TW80 in the TEL/TW80/COP formulation (Fig. 4), described and captured by the difference in η_0, the zero-shear

Table 2
Blend powder properties.

Formulation	Blend Bulk Density [g/mL]	Matrix PSD			Blend loss-on-drying [%]
		d_{10} [μm]	d_{50} [μm]	d_{90} [μm]	
10% TEL/COP	0.36	24.0 ± 0.4	79.3 ± 1.2	184 ± 1	0.86
10% TEL/5% TW80/COP	0.42	22.1 ± 0.3	81.3 ± 1.1	181 ± 0	1.26

Table 3
Carreau-Yasuda and WLF equation parameters for master curves at 170 °C reference temperature.

Formulation	10% TEL/5% TW80/COP	10% TEL/COP
T_0 [°C]	170	170
λ [s]	0.024	0.071
n	0.630	0.514
η_0 [Pa·s]	629.3	5134
η_∞ [Pa·s]	0	0
a	0.965	0.708
C_1	6.2	10.74
C_2 [°C]	146	190.2

rate viscosity (Table 3). The melt viscosity for both TEL formulations is a function of temperature (Fig. 4). The expected reduction in melt viscosity as temperature increases is seen for both formulations.

Another potentially interesting behavior is the slight difference in shear-thinning tendency, seen as the slope in the power law region of the melt viscosity profile and described by the power law index, n. The power law index is higher for the formulation with TW80 (Table 3), potentially indicating that this formulation is less susceptible to shear-thinning than the binary mixture. This observation and its effect on melt temperature evolution is further explored via a sensitivity analysis simulation study (see next section). Other differences include the variation of the Yasuda constant, a, and the characteristic time, λ. The observed range of the Yasuda constant results in a minor impact on the melt viscosity profile, namely the curvature of the transition region. In addition, within the shear rate range expected in the extruder, between 10 and 1000 1/s or rad/s and even up to 10,000 1/s at high screw speeds [52], depending on the screw clearance, the difference in λ can also be neglected because the processing region is almost fully in the power law region of the melt viscosity profile.

3.1.3.2. Ludovic® sensitivity analysis of shear-thinning, n, and plasticization, η_0, on melt temperature evolution. Sensitivity analysis of the rheological properties showed that η_0 has a higher impact on the melt temperature evolution than n, within the ranges of barrel temperature and screw speed tested (Fig. 5). At low barrel temperature, screw speed strongly impacted the melt temperature (higher ΔT_{max} values). At increasingly higher barrel temperatures, screw speed had a diminishing impact (lower ΔT_{max} values). Regardless of the processing condition, n impacted the melt temperature less than η_0 did, but the n or η_0 value corresponding to higher intrinsic melt viscosity led to higher melt temperature. In other words, high n and η_0 (blue diamonds) resulted in higher melt temperature while low n and η_0 (red triangles) resulted in lower melt temperature.

3.2. Experimental extrusion – Produce data to build and validate Ludovic® model

A laboratory extrusion experiment was conducted to investigate and quantify the relationship between processing parameters, formulation matrix composition and CQA, in this case residual crystallinity. All processing conditions yielded extrudates with measurable residual crystallinity. The amount of residual crystallinity depended on the matrix composition and on the processing conditions (Fig. 6). As expected, less residual crystallinity was observed with both higher temperatures and higher screw speeds. However, despite the same processing conditions being applied to both formulations, for all conditions, more residual crystallinity was observed in the formulations containing TW80. The die exit melt temperature increased with increasing barrel temperature and increasing screw speed, and were generally higher for the un-plasticized formulation, especially at lower barrel temperatures.

When all process conditions were analyzed by formulation, the residual crystallinity correlated strongly with the measured die-exit melt temperature (Fig. 7a). The linear regression equations for the two formulations were similar. The residual crystallinity varied more as a function of screw speed at lower barrel temperatures than at higher barrel temperatures. When the Ludovic® model was applied to simulate the laboratory extrusion experiments, utilizing the measured material property inputs given in Table 3 and Table 4, the simulated and measured die-exit melt temperatures were found to be strongly correlated across all formulations and process conditions (Fig. 7b), with regression equation given in the figure. Thus, the model was validated, showing that the 1D Ludovic® simulation software is capable of determining experimental extrusion process characteristics.

3.3. Process modeling – Use of the maximum melt temperature and viscous dissipation

Process modeling enabled analysis of the melt temperature inside the extruder, in particular the maximum temperature (Fig. 2), which is a difficult quantity to measure via typical temperature sensing methods. As was seen for the experimental melt temperature at die exit, the simulated maximum melt temperature increased with both increasing screw speed and increasing barrel temperature (Fig. 8a). At a screw speed of 400 rpm and barrel temperature of 200 °C, both formulations reached simulated max temperatures greater than the API solubility temperature of 10 %w/w TEL in the polymeric matrix, 213 °C. It was at these same processing conditions that almost no residual crystallinity was observed (Fig. 6 and symbols marked with an asterisk, *, in Fig. 8a). Little residual crystallinity, namely less than 0.5 %w/w, was also observed for the TEL/COP formulation processed at barrel temperature of 190 °C and screw speed of 400 rpm as well as for both

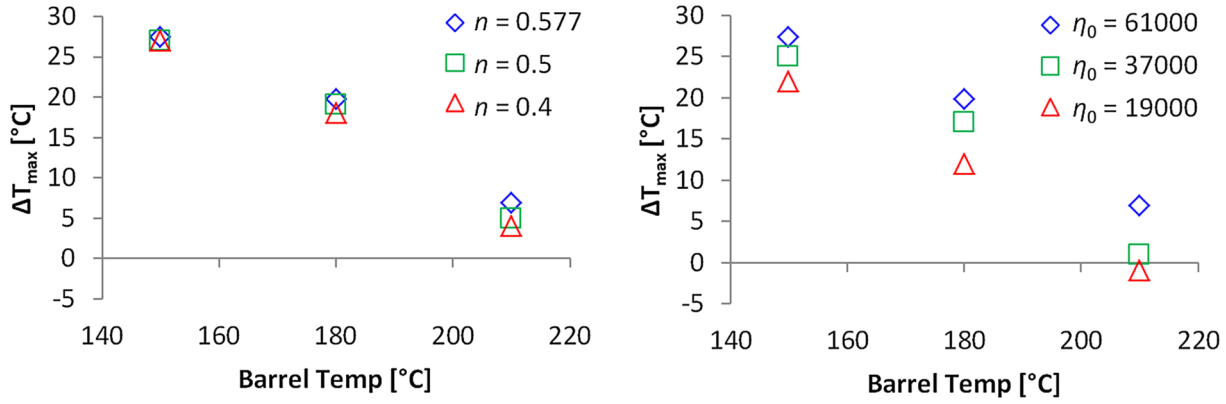

Fig. 5. Extent of simulated melt temperature rise as a function of screw speed (see Fig. 2 for explanation of ΔT_{max} and relationship to screw speed) for different main barrel temperature and values of n and η_0.

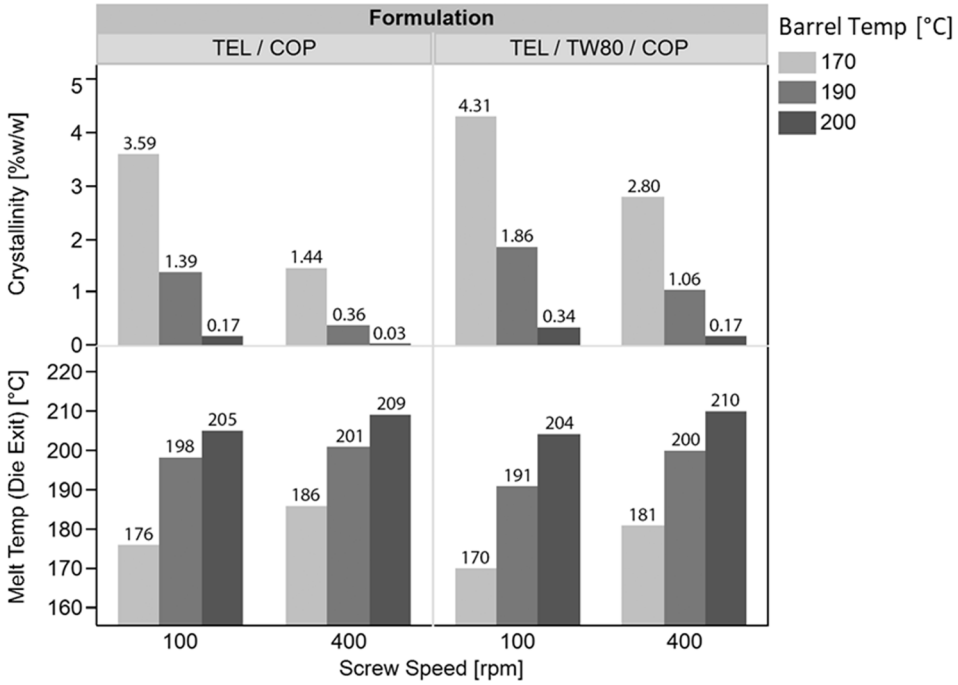

Fig. 6. Residual crystallinity in extrudate product and measured die-exit melt temperature.

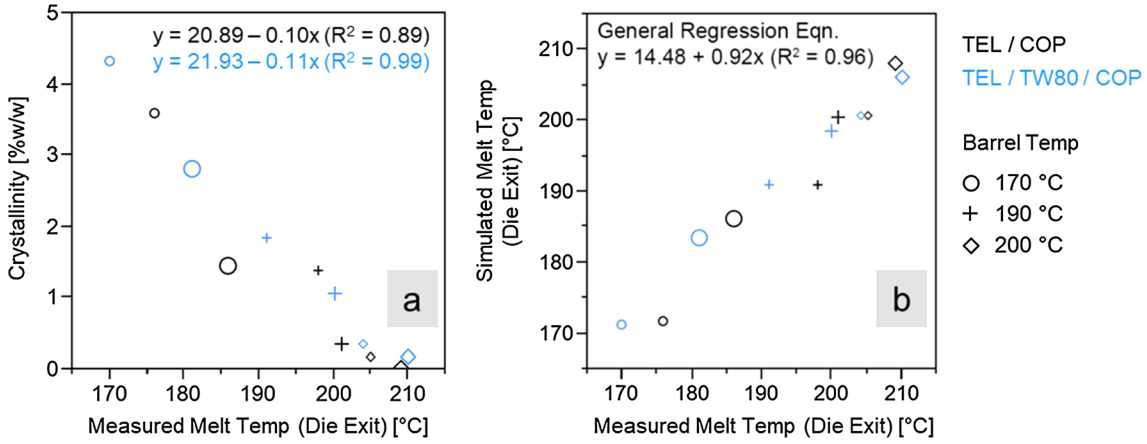

Fig. 7. Correlation of (a) residual crystallinity and measured die-exit melt temperature and (b) simulated and measured die-exit melt temperatures. Small symbols are for screw speeds of 100 rpm while large symbols are for 400 rpm.

Table 4
Material property inputs for simulation.

Formulation	TEL/TW80/COP	TEL/COP
Solid c_p (J/kg/°C)	1000	1000
Solid Density (kg/m^3)	400	400
Solid Thermal Conductivity (W/m·K)	0.19	0.19
Liquid c_p* (J/kg/°C)	f(T), at 170 °C = 1763	f(T), at 170 °C = 1822
Liquid Density (kg/m3)	1150	1150
Liquid Thermal Conductivity (W/m·K)	0.19	0.19
T_g as Melting Temperature (°C)	92	110
Melting Enthalpy (kJ/kg)	0	0

* In Ludovic® software, the liquid heat capacity c_p was entered as a function of temperature, data not shown.

formulations processed at barrel temperature of 200 °C but only 100 rpm screw speed. For the two formulations extruded at 200 °C and 100 rpm, the maximum melt temperature was slightly below the API solubility temperature. In comparison to the melt temperature measured at die exit (Fig. 6), a greater distinction can be made between the two formulations in the simulated maximum melt temperature in the extruder. Namely, for a given processing condition, a higher simulated maximum melt temperature was always observed for the un-plasticized TEL/COP formulation. Furthermore, as was seen with the viscosity parameter sensitivity analysis, the higher intrinsic viscosity formulation, TEL/COP, reached higher melt temperatures within the same range of screw speeds, independent of the barrel temperature setting (Fig. 8b). In addition, the screw speed sensitivity ΔT_{max} decreased for both formulations as barrel temperature was increased, corroborating the observations that residual crystallinity was less sensitive to changes in screw speed at higher temperatures.

The temperature rise, as a function of formulation and screw speed, is in part related to the total dissipated energy in the screw, a quantity accessible by simulation (Fig. 9). Higher values of dissipated energy were computed for the un-plasticized formulation TEL/COP than for the TEL/TW80/COP formulation for all processing conditions. For both formulations, higher screw speed generally led to higher dissipated

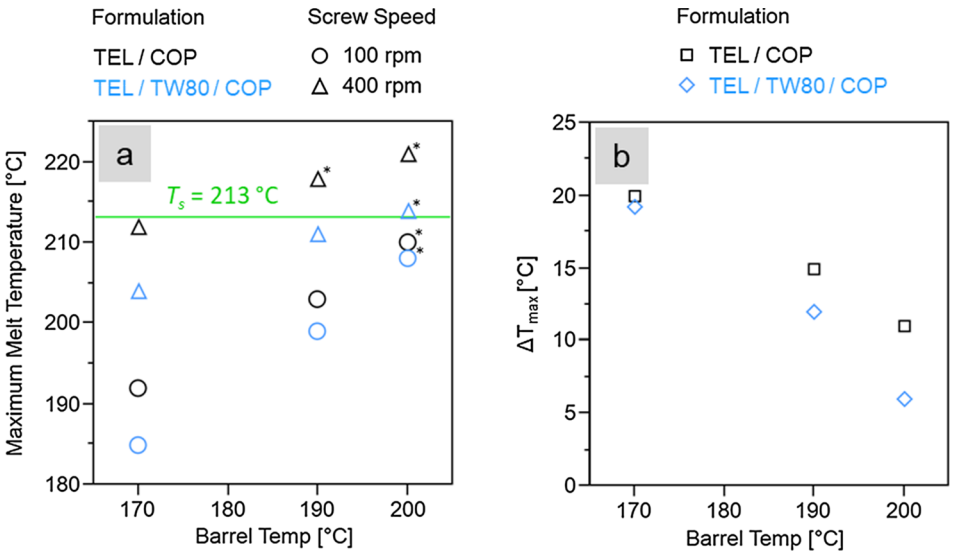

Fig. 8. Simulated maximum melt temperature (a) and extent of melt temperature rise as a function of screw speed ΔT_{max} (b) for different barrel temperatures and formulations. The API solubility temperature, T_s, for 10 %w/w TEL in the matrices is designated in (a) and extrudates with less than 0.5 %w/w residual crystallinity are indicated with an asterisk (*).

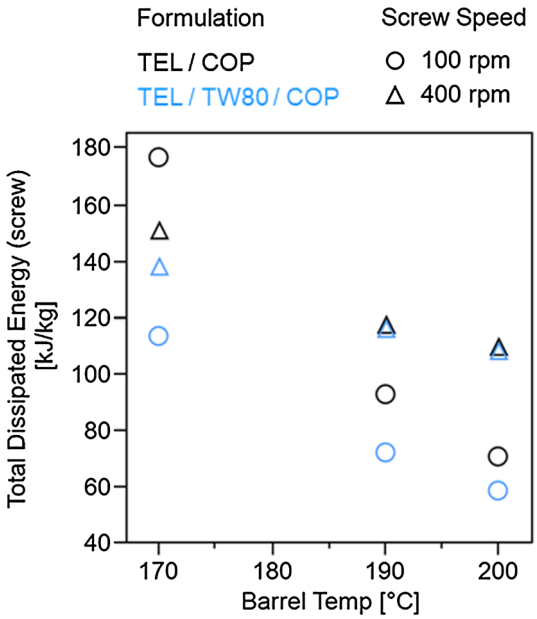

Fig. 9. Total dissipated energy from the screw as a function of processing condition and formulation.

energy, except for at the lowest temperature at which the lower screw speed yielded a higher dissipated energy.

4. Discussion

Telmisartan in copovidone is an informative model system for studying the relationship between formulation material properties and HME processing characteristics for ASD formation. Selection of the process parameters was informed by the API-polymer matrix solubility phase diagram so as to achieve a measurable level of the CQA, residual crystallinity. By processing near to or below TEL's solubility temperature at 10 %w/w, and far below its melting temperature of 269 °C, TEL dissolves incompletely into the polymer matrix. In addition, it is thermo-stable and exhibits non-plasticizing behavior at 10 %w/w drug loading in COP. With such material properties, the effect of the matrix melt viscosity on processing design space could be studied, with and without the addition of a plasticizing surfactant, TW80.

Several steps were carried out to ensure comparability of the two formulations. First, the TW80/COP matrix was pre-extruded in order to isolate the study of the dissolution of TEL into the already homogeneously plasticized matrix and facilitate comparison with the COP matrix formulation. Second, as a result of the prior processing of the TW80/COP matrix, the material was dehydrated, eliminating the plasticizing effect of moisture. Correspondingly, the COP raw material was also dehydrated. By dehydrating both matrices, the melt rheological behavior was simplified and made to be more similar with the material measured with the rheometer; in fact, rheological studies are most reliable when performed in the absence of water, especially in the temperature regions of interest here. Third, the pre-extruded TW80/COP matrix was milled to similar particle size distribution as the raw COP material with the intention of maintaining blend bulk density and therefore fill volume in the extruder constant. Further studies are needed to determine if these precautions were absolutely necessary.

One of the goals of this study was to evaluate the significance of melt rheology, in particular the plasticization and apparent shear-thinning behavior of a surfactant, on ASD formation. The formation of the ASD, namely the dissolution of the API, as measured by residual crystallinity, is a function of the independent process parameters, e.g. barrel temperature, screw speed, feed rate, as well as the resultant process performance, e.g. product temperature, melt viscosity, shear rate. However, the process performance is in turn dependent on the properties of the material being processed, e.g. matrix melt viscosity. These inter-dependent relationships were simultaneously considered using process simulation.

First, simulation was used to investigate the sensitivity of the melt temperature rise as a function of screw speed and barrel temperature for materials with different rheological characteristics, η_0 and n. Both of these parameters have been observed to vary from polymer to polymer and from formulation to formulation [34,11,80]. Depending on the shear rate range of the process, which is typically between 100 and 10,000 1/s [52], either or both of these parameters can influence the resulting melt viscosity. However, our results indicated that the overall plasticization described by η_0 is the dominating factor. Within the shear rate range explored, the melt viscosity profile essentially shifts vertically along the melt viscosity axis, with η_0 exhibiting a greater shift than n (Fig. 4). While intrinsic shear-thinning behavior described by n does contribute to melt viscosity reduction, decreased viscous dissipation and therefore lower heat rise, it was less substantial in this case. However, HME process simulations can and should be used to evaluate the relative significance of the viscosity parameters in other systems as well. This example also highlights the relevance of the model developed by the working group of K.G. Wagner to estimate melt viscosity by a straightforward T_g measurement [56,57,11], but also that further work

is needed to extend the model for matrices which exhibit different non-Newtonian behavior.

Second, simulation was used to retrospectively gain insight into the experimental results. After validating the model by obtaining correlation between the measured and simulated melt temperatures, the additional results that only simulation can produce, maximum melt temperature and viscous dissipated energy, were correlated with the CQA, residual crystallinity. In this way, process conditions and material properties were again simultaneously taken into consideration. Through analysis of the ΔT_{max}, melt temperature rise as a function of formulation melt viscosity, barrel temperature and screw speed showed that the design space as a function of screw speed is broader for the plasticized formulation. In this study, this behavior was shown with TW80 as a surfactant in COP, and in a related publication, we showed the same behavior with a sorbitan monolaurate/COP system [18].

Further, simulation revealed that the maximum melt temperature within the extruder was found to strongly correlate with residual crystallinity. Residual crystallinity approached zero as the simulated maximum melt temperature was close to the solubility temperature given by the API solubility phase diagram for the given drug loading, thus differentiating between the formulations with differing intrinsic melt viscosity. As Moseson and Taylor recently described theoretically and demonstrated practically, using a small conical twin-screw extruder, the thermodynamics and use of API-polymer matrix phase diagrams clearly and scientifically explain the requirement of reaching the solubility temperature for achieving a crystal-free ASD [36]. This argumentation of thermodynamic driving force for dissolution, the API solubility temperature, also explains the strong correlation between residual crystallinity, maximum melt temperature and the greater degree of TEL dissolution into the matrix for the un-plasticized TEL/COP formulation.

An increase in matrix temperature, regardless of the source, e.g. conduction from the barrels or from viscous dissipation, will increase the saturation solubility of the API and therefore the dissolution rate; this saturation solubility value is equivalent to the solubility temperature given in the phase diagram. In our case, the temperature rise, locally in the 2nd mixing zone, was higher for the formulation with higher intrinsic melt viscosity due to pronounced viscous dissipation. This heat rise was enough to increase the saturation solubility and induce more dissolution of the API in the un-plasticized system. However, at increasingly high barrel temperatures, the differences observed between the two formulations in maximum melt temperature and viscous dissipation diminished. These results were a direct reflection of the increasing similarity of the measured melt temperature and residual crystallinity between the two formulations at higher barrel temperatures.

Interestingly, the highest dissipated energy, observed for the un-plasticized formulation at 100 rpm and 170 °C (Fig. 9), did not directly translate into the highest melt temperature or lowest observed residual crystallinity. Here, the shear rate and melt temperature were so low that insufficient shear-thinning occurred, resulting in a high value for viscosity, leading to higher dissipated energy. However, this high viscous dissipation was not enough to overcome the predominant effect of temperature control by conduction from the barrels at this temperature setting. In addition, at this processing setting, the feed rate was relatively low, leading to longer residence times and correspondingly more time for melt temperature to equilibrate with that of the barrel wall. This type of result, highlighting different heat generation phenomena in different processing regimes, proves the value of process simulation due to consideration of all relationships between relevant material property and process parameter inputs simultaneously. Despite these interdependent relationships, the simulated maximum melt temperature still correlated with the CQA residual crystallinity.

The impact of the overall process time, that is residence time, on the CQA residual crystallinity can be inferred, as it was not independently varied. A longer residence time in the extruder can also lead to more observed dissolution. In this study, for a given combination of feed rate and screw speed, the residence time would have been shorter as a consequence of increasing feed rate proportionally to screw speed in order to maintain fill ratio for all conditions, consistent with published RTD characteristics for TSEs [81,82]. However, more residual crystallinity was observed with low feed rates, i.e. long residence times, and therefore this cannot be the dominating factor for dissolution of TEL. Of course, a separate study in which the temperature and residence time are independently varied could be performed to confirm this inference.

The reduced T_g of the TW80 formulation does not indicate an explanation for higher residual crystallinity. The potential for recrystallization post-extrusion at 10 %w/w TEL is low because the formulation T_g is 92 °C, well above the recommended 50 °C above room temperature [83]. In addition, the pure drug substance does not recrystallize from the amorphous state upon re-heating (data not included, see Lepek et al. [66]).

Despite the complex interdependent and simultaneously evolving relationships between all of the independent process and formulation parameters (e.g. screw speed, barrel temperature, feed rate, screw configuration, material properties) and process variables (e.g. melt temperature, shear rate, viscosity, residence time), which can in part be accounted for by use of process simulation, the strongest evidence for less observed residual crystallinity in the un-plasticized formulation is the generally higher material temperature. After all, the residual crystallinity approached 0 %w/w when the simulated maximum melt temperature reached the solubility temperature. For more dramatically evolving systems, for example when the API itself is a strong plasticizer for the matrix, process modeling may help to explain complex processing behavior. However, the same challenges as those mentioned by Vergnes and Berzin for modeling reactive extrusion will also apply to pharmaceutical HME [84] and will need to be addressed.

While the TW80 certainly exhibited the typical behavior of a plasticizer, that is decreasing the T_g and therefore overall viscosity profile, it also widened the design space with respect to screw speed. While traditional plasticizers such as solid state plasticizers can be expected to have the same effect, this behavior from a surfactant offers an additional justification for including a surfactant in an ASD formulation; beyond improving bioavailability enhancement [85], the surfactant can improve processability. Of course, traditional plasticizers are typically advised for decreasing the processing temperature to avoid high temperatures which could lead to API or polymer degradation [86,87]. However, our study shows that this would not help to achieve complete dissolution due to lack of a thermodynamic driving force, as has been suggested by others [37,36]. Instead, process conditions must induce a melt temperature which reaches the API solubility temperature for the given drug load.

5. Conclusions

Telmisartan in copovidone is an informative model system for the study of HME Quality-by-Design. It enabled the comprehensive evaluation of the relationship between formulation material properties and HME processing characteristics for ASD formation. Due to its high solubility temperature and non-plasticizing characteristic in copovidone-based polymer matrices at a concentration of 10 %w/w, the plasticizing effect of a common surfactant on the HME process could be isolated and studied. While surfactants are commonly selected to enhance the bioavailability of a drug substance, we found that the plasticizing behavior of polysorbate 80 broadened the processing design space with respect to screw speed. Also, while plasticizers are commonly incorporated to reduce the processing temperature, we also found that by doing so in the case of TEL with a high API solubility temperature, the complete formation of the ASD was hindered; complete reduction of residual crystallinity is only possible if the melt temperature reaches the thermodynamic API solubility temperature. Therefore, a temperature increase in kneading blocks due to viscous dissipation generated by a

highly viscous melt was required to achieve a fully amorphous system. Process simulations, in which matrix viscosity, screw speed and barrel temperature were varied, enabled simultaneous consideration of the complex inter-dependent relationships inherent to HME, namely those between formulation material properties, independent process parameters, and process dependent variables such as melt temperature and viscosity and their impact on the CQA residual crystallinity. In this way, the measured melt temperature and simulated maximum melt temperature were correlated with residual crystallinity, differentiating the process behavior between plasticized and un-plasticized matrices. For TEL in these copovidone-based polymer matrices specifically, a design space within which various combinations of independent process variables yield a maximum melt temperature greater than the solubility temperature of 213 °C can be expected to produce a crystal-free extrudate. Of course, processing at elevated temperatures too far above the solubility temperature should be considered in the context of balancing the risk between achieving a crystal-free extrudate and avoiding thermal degradation of the formulation components.

Acknowledgements

The authors wish to thank Dirk Remmler, Ekaterina Sobich, Teresa Dagenbach, Amelie Wirth, Max Frentzel, Ute Lander, Constanze Schmidt, Mirko Pauli, David Gessner and Stefan Weber of AbbVie Deutschland GmbH & Co. KG for their support in conducting experiments and Kristin Lehmkemper and Thomas Kessler of AbbVie for helpful and productive discussions.

Disclosures

Rachel C. Evans, Esther S. Bochmann, Samuel O. Kyerematen and Andreas Gryczke are employees of AbbVie and may own AbbVie stock options. Karl G. Wagner is an employee of the University of Bonn. Esther S. Bochmann was an employee of the University of Bonn when work was conducted. AbbVie sponsored and funded the study; contributed to the design; participated in the collection, analysis, and interpretation of data, and in writing, reviewing, and approval of the final publication.

Appendix A. Supplementary material

Supplementary data to this article can be found online at https://doi.org/10.1016/j.ejpb.2019.05.021.

References

[1] J. Breitenbach, Melt extrusion: from process to drug delivery technology, Eur. J. Pharm. Biopharm. 54 (2) (2002) 107–117.
[2] M.A. Repka, S. Bandari, V.R. Kallakunta, A.Q. Vo, H. McFall, M.B. Pimparade, et al., Melt extrusion with poorly soluble drugs – An integrated review, Int. J. Pharm. 535 (1) (2018) 68–85.
[3] S.V. Jermain, C. Brough, R.O. Williams, Amorphous solid dispersions and nanocrystal technologies for poorly water-soluble drug delivery – An update, Int. J. Pharm. 535 (1) (2018) 379–392.
[4] M.A. Repka, N. Langley, J. DiNunzio, Melt extrusion. first ed. New York: Springer-Verlag, 2013. 474 p. (AAPS Advances in the Pharmaceutical Sciences; vol. 9).
[5] Changquan Calvin Sun, Materials science tetrahedron—A useful tool for pharmaceutical research and development, J. Pharm. Sci. 98 (5) (2008) 1671–1687.
[6] T. Vigh, G. Drávavölgyi, P.L. Sóti, H. Pataki, T. Igricz, I. Wagner, et al., Predicting final product properties of melt extruded solid dispersions from process parameters using Raman spectrometry, J. Pharm. Biomed. Anal. 98 (2014) 166–177.
[7] A. Gryczke, Hot-melt extrusion process design using process analytical technology. In: Melt extrusion, first ed. New York: Springer-Verlag, 2013. (AAPS Advances in the Pharmaceutical Sciences; vol. 9).
[8] C. Brown, J. DiNunzio, M. Eglesia, S. Forster, M. Lamm, M. Lowinger, Hot-melt extrusion for solid dispersions: composition and design considerations, in: N. Shah, H. Sandhu, D.S. Choi, H. Chokshi, A.W. Malick (Eds.), Amorphous Solid Dispersions: Theory and Practice [Internet], Springer New York, New York, NY, 2014, pp. 197–230, , https://doi.org/10.1007/978-1-4939-1598-9_6.
[9] J. Aho, J.P. Boetker, S. Baldursdottir, J. Rantanen, Rheology as a tool for evaluation of melt processability of innovative dosage forms, Potential 2D 3D Print Pharm. Dev. 494 (2) (2015) 623–642.
[10] S.-Y. Chan, S. Qi, D.Q.M. Craig, An investigation into the influence of drug–polymer interactions on the miscibility, processability and structure of polyvinylpyrrolidone-based hot melt extrusion formulations, Spec. Issue Contin. Manuf. Process. Anal. Tools 496 (1) (2015) 95–106.
[11] E.S. Bochmann, E.E. Üstüner, A. Gryczke, K.G. Wagner, Predicting melt rheology for hot-melt extrusion by means of a simple Tg-measurement, Eur. J. Pharm. Biopharm. 119 (Oct) (2017) 47–55.
[12] K. Kachrimanis, I. Nikolakakis, Polymers as formulation excipients for hot-melt extrusion processing of pharmaceuticals, Handbook of Polymers for Pharmaceutical Technologies, Scrivener Publishing LLC, 2015, pp. 121–150.
[13] S.S. Gupta, T. Parikh, A.K. Meena, N. Mahajan, I. Vitez, A.T.M. Serajuddin, Effect of carbamazepine on viscoelastic properties and hot melt extrudability of Soluplus®, Int. J. Pharm. 478 (1) (2015) 232–239.
[14] F. Yang, Y. Su, L. Zhu, C.D. Brown, L.A. Rosen, K.J. Rosenberg, Rheological and solid-state NMR assessments of copovidone/clotrimazole model solid dispersions, Int. J. Pharm. 500 (1) (2016) 20–31.
[15] M.A. Repka, T.G. Gerding, S.L. Repka, J.W. McGinity, Influence of plasticizers and drugs on the physical-mechanical properties of hydroxypropylcellulose films prepared by hot melt extrusion, Drug Dev. Ind. Pharm. 25 (5) (1999) 625–633.
[16] D. Desai, H. Sandhu, N. Shah, W. Malick, H. Zia, W. Phuapradit, et al., Selection of solid-state plasticizers as processing aids for hot-melt extrusion, J. Pharm. Sci. 107 (1) (2018) 372–379.
[17] J. Aho, J. Van Renterghem, L. Arnfast, T. De Beer, J. Rantanen, The flow properties and presence of crystals in drug-polymer mixtures: Rheological investigation combined with light microscopy, Int. J. Pharm. 528 (1) (2017) 383–394.
[18] R.C. Evans, S.O. Kyerematen, M. Degenhardt, K.G. Wagner, Influence of Surfactant +Polymer rheological properties on hot-melt extrusion design space - investigation via process simulation, APV International Association for Pharmaceutical Technology, Granada, Spain, 2018.
[19] G. Verreck, A. Decorte, H. Li, D. Tomasko, A. Arien, J. Peeters, et al., The effect of pressurized carbon dioxide as a plasticizer and foaming agent on the hot melt extrusion process and extrudate properties of pharmaceutical polymers, J. Supercrit. Fluids. 38 (3) (2006) 383–391.
[20] A.N. Ghebremeskel, C. Vemavarapu, M. Lodaya, Use of surfactants as plasticizers in preparing solid dispersions of poorly soluble API: stability testing of selected solid dispersions, Pharm. Res. 23 (8) (2006) 1928–1936.
[21] A.N. Ghebremeskel, C. Vemavarapu, M. Lodaya, Use of surfactants as plasticizers in preparing solid dispersions of poorly soluble API: Selection of polymer–surfactant combinations using solubility parameters and testing the processability, Int. J. Pharm. 328 (2) (2007) 119–129.
[22] C. De Brabander, G. van den Mooter, C. Vervaet, J.P. Remon, Characterization of ibuprofen as a nontraditional plasticizer of ethyl cellulose, J. Pharm. Sci. 91 (7) (2002) 1678–1685.
[23] M.A. Repka, J.W. McGinity, Influence of Vitamin E TPGS on the properties of hydrophilic films produced by hot-melt extrusion, Int. J. Pharm. 202 (1) (2000) 63–70.
[24] C. Wu, J.W. McGinity, Non-traditional plasticization of polymeric films, Int. J. Pharm. 177 (1) (1999) 15–27.
[25] M. Yang, P. Wang, H. Suwardie, C. Gogos, Determination of acetaminophen's solubility in poly(ethylene oxide) by rheological, thermal and microscopic methods, Int. J. Pharm. 403 (1–2) (2011) 83–89.
[26] F. Siepmann, V. Le Brun, J. Siepmann, Drugs acting as plasticizers in polymeric systems: A quantitative treatment, J. Controlled Release. 115 (3) (2006) 298–306.
[27] C. Wu, J.W. McGinity, Influence of ibuprofen as a solid-state plasticizer in eudragit® RS 30 D on the physicochemical properties of coated beads, AAPS Pharm.Sci.Tech. 2 (4) (2001) 35–43.
[28] Y. Zhu, N.H. Shah, A.W. Malick, M.H. Infeld, J.W. McGinity, Solid-state plasticization of an acrylic polymer with chlorpheniramine maleate and triethyl citrate, Int. J. Pharm. 241 (2) (2002) 301–310.
[29] R.J. Chokshi, H.K. Sandhu, R.M. Iyer, N.H. Shah, A.W. Malick, H. Zia, Characterization of physico-mechanical properties of indomethacin and polymers to assess their suitability for hot-melt extrusion processs as a means to manufacture solid dispersion/solution, J. Pharm. Sci. 94 (11) (2005) 2463–2474.
[30] Mayur S. Dudhedia, Anjali M. Agrawal, Rheological study of copovidone and solid dispersion blend used for hot melt extrusion, J. Appl. Polym. Sci. [Internet] 133 (14) (2015), https://doi.org/10.1002/app.43278.
[31] F. Yang, Y. Su, J. Zhang, J. DiNunzio, A. Leone, C. Huang, et al., Rheology guided rational selection of processing temperature to prepare copovidone-nifedipine amorphous solid dispersions via Hot Melt Extrusion (HME), Mol. Pharm. 13 (10) (2016) 3494–3505.
[32] D.E. Zecevic, K.G. Wagner, Rational development of solid dispersions via hot-melt extrusion using screening, material characterization, and numeric simulation tools, J. Pharm. Sci. 102 (7) (2013) 2297–2310.
[33] N. Solanki, S.S. Gupta, A.T.M. Serajuddin, Rheological analysis of itraconazole-polymer mixtures to determine optimal melt extrusion temperature for development of amorphous solid dispersion, Eur. J. Pharm. Sci. 1 (111) (2018) 482–491.
[34] A.L. Sarode, H. Sandhu, N. Shah, W. Malick, H. Zia, Hot melt extrusion (HME) for amorphous solid dispersions: Predictive tools for processing and impact of drug–-polymer interactions on supersaturation, Eur. J. Pharm. Sci. 48 (3) (2013) 371–384.
[35] R. Dukeck, P. Sieger, P. Karmwar, Investigation and correlation of physical stability, dissolution behaviour and interaction parameter of amorphous solid dispersions of telmisartan: A drug development perspective, Eur. J. Pharm. Sci. 49 (4) (2013) 723–731.
[36] D.E. Moseson, L.S. Taylor, The application of temperature-composition phase diagrams for hot melt extrusion processing of amorphous solid dispersions to prevent

residual crystallinity, Int. J. Pharm. 553 (1) (2018) 454–466.
[37] N. Boersen, C. Brown, J. DiNunzio, D. Johnson, P. Marsac, R. Meyer, Hot-Melt Extrusion: The Process-Product-Performance Interplay, in: A.C. Templeton, S.R. Byrn, R.J. Haskell, T.E. Prisinzano (Eds.), Discovering and Developing Molecules with Optimal Drug-Like Properties [Internet], Springer New York, New York, NY, 2015, pp. 345–381, , https://doi.org/10.1007/978-1-4939-1399-2_11.
[38] Pharmaceutical Development Annex to Q8(R2) [Internet]. ICH; 2009. Available from: http://www.ich.org/fileadmin/Public_Web_Site/ICH_Products/Guidelines/Quality/Q8_R1/Step4/Q8_R2_Guideline.pdf.
[39] D.M. Kremer, B.C. Hancock, Process simulation in the pharmaceutical industry: A review of some basic physical models, J. Pharm. Sci. 95 (3) (2006) 517–529.
[40] J. Markarian, Compounders look to simulation software for savings in time and costs, Plast. Addit. Compd. 7 (2) (2005) 34–37.
[41] B. Vergnes, G.D. Valle, L. Delamare, A global computer software for polymer flows in corotating twin screw extruders, Polym. Eng. Sci. 38 (11) (1998) 1781–1792.
[42] H. Potente, M. Bastian, J. Flecke, Design of a compounding extruder by means of the SIGMA simulation software, Adv. Polym. Technol. 18 (2) (1999) 147–170.
[43] J.L. White, J. Keum, H. Jung, K. Ban, S. Bumm, Corotating twin-screw extrusion reactive extrusion-devolatilization model and software, Polym.-Plast. Technol. Eng. 45 (4) (2006) 539–548.
[44] I. Banu, J.-P. Puaux, G. Bozga, I. Nagy, Modeling of L-lactide polymerization by reactive extrusion, Macromol. Symp. 289 (1) (2010) 108–118.
[45] A. Farahanchi, M.J. Sobkowicz, Kinetic and process modeling of thermal and mechanical degradation in ultrahigh speed twin screw extrusion, Polym. Degrad. Stab. 1 (138) (2017) 40–46.
[46] P.S. Dubey, A.H. Abhyankar, V. Marchante, L.J. Brighton, K. Blackburn, C. Temple, et al., Modelling and validation of synthesis of poly lactic acid using an alternative energy source through a continuous reactive extrusion process, Polymers 8 (4) (2016).
[47] O.S. Carneiro, J.A. Covas, B. Vergnes, Experimental and theoretical study of twin-screw extrusion of polypropylene, J. Appl. Polym. Sci. 78 (7) (2000) 1419–1430.
[48] F. Berzin, A. Tara, L. Tighzert, B. Vergnes, Importance of coupling between specific energy and viscosity in the modeling of twin screw extrusion of starchy products, Polym. Eng. Sci. 50 (9) (2010) 1758–1766.
[49] F. Berzin, A. Tara, L. Tighzert, B. Vergnes, Computation of starch cationization performances by twin-screw extrusion, Polym. Eng. Sci. 47 (2) (2007) 112–119.
[50] N. Balakrishnan, Validation of residence stress distribution methodology using 1-D computer simulations (Master of Science). (College Park): University of Maryland.
[51] M.A. Emin, Modeling extrusion processes, Available from: in: S. Bakalis, K. Knoerzer, P.J. Fryer (Eds.), Modeling Food Processing Operations [Internet], Woodhead Publishing, 2015, pp. 235–253.
[52] K. Kohlgrüber, Co-rotating twin-screw extruders - fundamentals, technology and applications, Carl Hanser Verlag, Munich, 2008.
[53] A. Redl, M.H. Morel, J. Bonicel, B. Vergnes, S. Guilbert, Extrusion of wheat gluten plasticized with glycerol: influence of process conditions on flow behavior, rheological properties, and molecular size distribution, Cereal Chem. 76 (3) (1999) 361–370.
[54] T. Domenech, E. Peuvrel-Disdier, B. Vergnes, The importance of specific mechanical energy during twin screw extrusion of organoclay based polypropylene nanocomposites, Compos. Sci. Technol. 11 (75) (2013) 7–14.
[55] D.E. Zecevic, R.C. Evans, K. Paulsen, K.G. Wagner, From benchtop to pilot scale–experimental study and computational assessment of a hot-melt extrusion scale-up of a solid dispersion of dipyridamole and copovidone, Int. J. Pharm. 537 (1) (2018) 132–139.
[56] E.S. Bochmann, K.E. Steffens, A. Gryczke, K.G. Wagner, Numerical simulation of hot-melt extrusion processes for amorphous solid dispersions using model-based melt viscosity, Eur. J. Pharm. Biopharm. 1 (124) (2018) 34–42.
[57] E. Bochmann, A. Gryczke, K. Wagner, Validation of model-based melt viscosity in hot-melt extrusion numerical simulation, Pharmaceutics 10 (3) (2018).
[58] A. Eitzlmayr, G. Koscher, G. Reynolds, Z. Huang, J. Booth, P. Shering, et al., Mechanistic modeling of modular co-rotating twin-screw extruders, Int. J. Pharm. 474 (1–2) (2014) 157–176.
[59] A. Eitzlmayr, J. Khinast, G. Hörl, G. Koscher, G. Reynolds, Z. Huang, et al., Experimental characterization and modeling of twin-screw extruder elements for pharmaceutical hot melt extrusion, AIChE J. 59 (11) (2013) 4440–4450.
[60] A. Eitzlmayr, J. Matić, J. Khinast, Analysis of flow and mixing in screw elements of corotating twin-screw extruders via SPH, AIChE J. 63 (6) (2016) 2451–2463.
[61] A. Eitzlmayr, J. Khinast, Co-rotating twin-screw extruders: Detailed analysis of conveying elements based on smoothed particle hydrodynamics. Part 1: Hydrodynamics, Chem. Eng. Sci. 29 (134) (2015) 861–879.
[62] A. Eitzlmayr, J. Khinast, Co-rotating twin-screw extruders: Detailed analysis of conveying elements based on smoothed particle hydrodynamics. Part 2 Mixing, Chem. Eng. Sci. 29 (134) (2015) 880–886.
[63] E. Reitz, H. Podhaisky, D. Ely, M. Thommes, Residence time modeling of hot melt extrusion processes, Eur. J. Pharm. Biopharm. 85 (3, Part B) (2013) 1200–1205.
[64] A. Schittny, H. Ogawa, J. Huwyler, M. Puchkov, A combined mathematical model linking the formation of amorphous solid dispersions with hot-melt-extrusion process parameters, Eur. J. Pharm. Biopharm. 1 (132) (2018) 127–145.
[65] R.C. Evans, S.O. Kyeremateng, L. Asmus, M. Degenhardt, J. Rosenberg, K.G. Wagner, Development and performance of a highly sensitive model formulation based on torasemide to enhance hot-melt extrusion process understanding and process development, AAPS Pharm.Sci.Tech. [Internet] (2018), https://doi.org/10.1208/s12249-018-0970-y.
[66] P. Lepek, W. Sawicki, K. Wlodarski, Z. Wojnarowska, M. Paluch, L. Guzik, Effect of amorphization method on telmisartan solubility and the tableting process, Eur. J. Pharm. Biopharm. 83 (1) (2013) 114–121.
[67] S. Jamadar, Y. Pore, F. Sayyad, Formation of amorphous telmisartan polymeric microparticles for improvement of physicochemical characteristics, Part. Sci. Technol. 32 (5) (2014) 512–519.
[68] S.O. Kyeremateng, M. Pudlas, G.H. Woehrle, A fast and reliable empirical approach for estimating solubility of crystalline drugs in polymers for hot melt extrusion formulations, J. Pharm. Sci. 103 (9) (2014) 2847–2858.
[69] T.G. Fox, Influence of diluent and of copolymer composition on the glass temperature of a polymer system, Bulletin of the American Physical Society, American Physical Society, New York City, 1956.
[70] K. Kolter, M. Karl, A. Gryczke, Hot-melt extrusion with BASF pharma polymers, second ed., BASF SE, Ludwigshafen, Germany, 2012.
[71] J.E. Mark, Physical properties of polymers handbook, second ed., Springer Science +Business Media, LLC, New York, 2007.
[72] D. Treffer, A. Troiss, J. Khinast, A novel tool to standardize rheology testing of molten polymers for pharmaceutical applications, Int. J. Pharm. 495 (1) (2015) 474–481.
[73] E.S. Bochmann, D. Neumann, A. Gryczke, K.G. Wagner, Micro-scale prediction method for API-solubility in polymeric matrices and process model for forming amorphous solid dispersion by hot-melt extrusion, Eur. J. Pharm. Biopharm. 107 (2016) 40–48.
[74] W.P. Cox, E.H. Merz, Rheology of polymer melts - A correlation of dynamic and steady flow measurements, in: Committee D-20Committee D-20 (Ed.), Int. Symp. Plast Test Stand [Internet], ASTM International, 100 Barr Harbor Drive, PO Box C700, West Conshohocken, PA 19428-2959, 1959, , https://doi.org/10.1520/STP44206S.
[75] P.J. Carreau, Rheological Equations from Molecular Network Theories, [Ph.D. thesis] University of Wisconsin, Madison, [Madison, Wisconsin], 1968.
[76] K. Yasuda, Investigation of the analogies between viscometric and linear viscoelastic properties of polystyrene fluids (Ph.D. thesis). (Cambridge): MIT.
[77] J. Vlachopoulos, N. Polychronopoulos, Basic concepts in polymer melt rheology and their importance in processing, Applied Polymer Rheology: Polymeric Fluids with Industrial Applications, first ed., John Wiley & Sons, Ltd, 2012, pp. 1–26.
[78] M.L. Williams, R.F. Landel, J.D. Ferry, The temperature dependence of relaxation mechanisms in amorphous polymers and other glass-forming liquids, J. Am. Chem. Soc. 77 (1955) 3701–3707.
[79] J.R. Fried, Polymer science and technology, second ed., Prentice Hall, New Jersey, 2003.
[80] S.M. Maru, M. de Matas, A. Kelly, A. Paradkar, Characterization of thermal and rheological properties of zidovidine, lamivudine and plasticizer blends with ethyl cellulose to assess their suitability for hot melt extrusion, Eur. J. Pharm. Sci. 44 (4) (2011) 471–478.
[81] A. Poulesquen, B. Vergnes, A study of residence time distribution in co-rotating twin-screw extruders. Part I: Theoretical modeling, Polym Eng Sci. 7, 43(12) (2004 Apr) 1841–1848.
[82] J. Puaux, G. Bozga, A. Ainser, Residence time distribution in a corotating twin-screw extruder, Chem. Eng. Sci. 55 (9) (2000) 1641–1651.
[83] B.C. Hancock, S.L. Shamblin, G. Zografi, Molecular mobility of amorphous pharmaceutical solids below their glass transition temperatures, Pharm. Res. 12 (6) (1995) 799–806.
[84] B. Vergnes, F. Berzin, Modeling of reactive systems in twin-screw extrusion: challenges and applications, Modif Dégrad Stabilisation PolymèresPolymer Modif Degrad Stabilisation. 9 (11–12) (2006) 1409–1418.
[85] J.C. DiNunzio, D.A. Miller, Formulation development of amorphous solid dispersions prepared by melt extrusion. In: Melt Extrusion, first ed. New York: Springer-Verlag, 2013. (AAPS Advances in the Pharmaceutical Sciences; vol. 9).
[86] G. Verreck, The influence of plasticizers in hot-melt extrusion, Available from: Hot-Melt Extrusion: Pharmaceutical Applications [Internet], John Wiley & Sons, Ltd, 2012, pp. 93–112.
[87] J.S. LaFountaine, J.W. McGinity, R.O. Williams, Challenges and strategies in thermal processing of amorphous solid dispersions: A review, AAPS Pharm.Sci.Tech. 17 (1) (2016) 43–55.